PCCP

PAPER

View Article Online
View Journal | View Issue

Cite this: *Phys. Chem. Chem. Phys.*, 2014, **16**, 12014

Improving $BiVO_4$ photoanodes for solar water splitting through surface passivation†

Yongqi Liang* and Johannes Messinger

Received 14th February 2014,
Accepted 1st May 2014

DOI: 10.1039/c4cp00674g

www.rsc.org/pccp

$BiVO_4$ has shown great potential as a semiconductor photoanode for solar water splitting. Significant improvements made during recent years allowed researchers to obtain a photocurrent density of up to 4.0 mA cm^{-2} (AM1.5 sunlight illumination, 1.23 V_{RHE} bias). For further improvements of the $BiVO_4$ photoelectrodes, a deep understanding of the processes occurring at the $BiVO_4$–H_2O interface is crucial. Employing an electrochemical loading and removal process of NiO_x, we show here that carrier recombination at this interface strongly affects the photocurrents. The removal of NiO_x species by electrochemical treatment in a phosphate electrolyte leads to significantly increased photocurrents for $BiVO_4$ photoelectrodes. At a bias of 1.23 V_{RHE}, the Incident Photon-to-Current Efficiency (IPCE) at 450 nm reaches 43% for the passivated $BiVO_4$ electrode under back side illumination. A model incorporating heterogeneity of NiO_x centers on the $BiVO_4$ surface (OER catalytic centers, recombination centers, and passivation centers) is proposed to explain this improved performance.

Introduction

With a photocurrent onset potential of <0.2 V_{RHE}, and a photocurrent of 7.0 mA cm^{-2} under AM1.5 solar light irradiation, $BiVO_4$ is predicted to be an efficient photoelectrode material for solar water splitting.[1–3] Very recently, it was shown that a photocurrent as high as 4.0 mA cm^{-2} can be achieved using $BiVO_4$ thin film electrodes.[1] However, low photocurrent densities (<1.0 mA cm^{-2} at 1.23 V_{RHE}) and high onset potentials for photocurrent (>0.6 V_{RHE})[3] are frequently reported. Further improvements are needed before the full potential of $BiVO_4$ can be reached for artificial leaf devices.[1,4]

To improve light-driven water splitting at $BiVO_4$ surfaces, various material properties such as bulk recombination,[1,5] electron transport[6,7] and the electron transfer across the interfaces[6,8] need to be optimized. Attempts have been made for $BiVO_4$ photoelectrodes to address these factors separately.[3,9] To improve the electron transfer across the oxide–water interface loading of the oxygen-evolution-reaction (OER) catalyst NiO_x/CoO_x onto the photoelectrodes has been under intensive research.[10–12] Though the performance improvements after CoO_x loading are verified in various oxide photoelectrodes, discussions arose recently[13] whether the improvements are due to the catalytic effects of CoO_x[14] or rather due to facilitating charge separation across the newly formed junction between the CoO_x layer and the photoelectrodes.[15] Here we demonstrate the influence of surface recombination on the performance of $BiVO_4$ photoelectrodes and show that a heterogeneity exists within the amorphous NiO_x layer loaded onto the $BiVO_4$ surface. We elucidate this heterogeneity by selectively removing the catalytic NiO_x species from the $BiVO_4$ surface for OER without affecting the NiO_x species that minimizes the surface recombination.

Experimental section

$BiVO_4$ films on FTO glass substrates (TEC15, Hartford) were prepared by following a reported procedure. Their Raman spectra show identical features to that reported previously. The SnO_2 interfacial layer was deposited in between $BiVO_4$ and FTO to improve the electron collection at the back contact.[6]

NiO_x loading onto $BiVO_4$ was carried out electrochemically according to a well-established method,[16] and the formula of MO_x (NiO_x and CoO_x) is used here to indicate the non-stoichiometric nature of the metal oxide–hydroxide layer deposited by this method. 1 mM $Ni(NO_3)_2{\cdot}6H_2O$ (98%, Alfa-Aesar) was mixed with 0.1 M borate buffered aqueous electrolyte (NaB*i*) at pH = 10.0, and the precipitate was removed from the solution using a syringe filter (0.2 μm pore size membranes) after aging the solution in air for ~20 min. The removal of NiO_x from the $BiVO_4$ surface was performed in a 0.2 M phosphate buffered aqueous electrolyte (NaP*i*) at pH = 7.0.

Departement of Chemistry, Kemiskt Biologiskt Centrum (KBC), Umeå Universitet, Linnaeus väg 6, S-901 87 Umeå, Sweden. E-mail: yongqi.liang@chem.umu.se

† Electronic supplementary information (ESI) available: The reflection spectrum of the mirror for the illumination setup, the CVs for the characterization of $BiVO_4$ films in NaP*i* and NaB*i*, the light transmission spectrum of the $BiVO_4$ film, the CVs for NiO_x loading and removal onto the FTO substrate, the XPS spectra of $BiVO_4$ films, and comparison of the photoresponse of $BiVO_4$ with/without the sulfite hole scavenger. See DOI: 10.1039/c4cp00674g

The photoelectrochemical characterization was carried out in 0.2 M NaB*i* at pH = 10.0. The potential of the $BiVO_4$ working electrode (0.283 cm^2) was controlled *via* a potentiostat (Autolab PG302N). A Ag/AgCl (3 M NaCl) electrode and a coiled Pt wire were used as the reference electrode (RE) and the counter electrode (CE) for the 3-electrode measurement, respectively. All the potentials in this paper were translated to the Reversible Hydrogen Electrode (RHE) scale by assuming the Nernstian behaviour for the oxide surfaces in aqueous solution. Unless mentioned otherwise, a scan rate of 50 mV s^{-1} was used. The anodic scan is referred to as forward scan, and the cathodic scan is referred as reverse scan. An AM1.5 solar simulator (Sol3A, model 94043A, Newport) was used as the light source during PEC characterization. A UV-enhanced mirror (PAUV-PM-5010M-C, Melles Griot) with close-to-flat response across the whole spectrum ($\sim$85% between 300 nm to 600 nm, $\sim$96% for $>$1000 nm, Fig. S1, ESI†) was employed to flip the simulated sunlight from the vertical to the horizontal direction. The photons go through the FTO substrate before they reach the $BiVO_4$ film first for back side illumination, while the photons need to penetrate the electrolyte before they reach the $BiVO_4$ film for front side illumination.[17] The light intensity (100 mW cm^{-2}) reaching the sample was calibrated using a thermopile detector (S302C, Thorlabs). For illumination at individual wavelengths, the white light from a tungsten-halogen lamp was dispersed through a monochromator (SpectraPro 2150, Acton). The second- or higher-order harmonics of light passing through the monochromator were removed using suitable long-pass filters (Schott). The light intensity of the photons at wavelengths from 300 nm to 600 nm was measured using a calibrated Si photodiode (PD300-UV, Ophir).

The high resolution XPS spectra of the $BiVO_4$ samples were recorded *via* a Kratos Axis Ultra electron spectrometer equipped with a delay line detector. A monochromatic Al Kα radiation source operated at 150 W, a hybrid lens system with a magnetic lens, and a charge neutralizer were used for all measurements. The resulting spectra were processed using the Kratos software and background-corrected using a Shirley background. All peak positions for the spectra recorded at room temperature were shifted against the C 1s peak at 285.0 eV. The spectra were determined from averaged values obtained over an analysis area of 0.3 mm $\times$ 0.7 mm^2 and pertained to an analysis depth of about 6 nm.

Results

Fig. 1 shows the performance of an as-prepared $BiVO_4$ photoelectrode. Both the CVs for the $BiVO_4$ electrode in the dark and under AM1.5 sunlight (front side illumination) were collected. The CV for the photoelectrode under AM1.5 sunlight illumination serves as the action curve. Since no characteristic parameter set (such as V_{oc}, I_{sc}, and fill factor for a photovoltaic device) is defined for photoelectrodes as yet, we take in this article the photocurrent under 1.23 V_{RHE} and the potential where the photocurrent curve crosses the potential-axis (the onset potential) as the criteria to compare the performances of $BiVO_4$ electrodes.

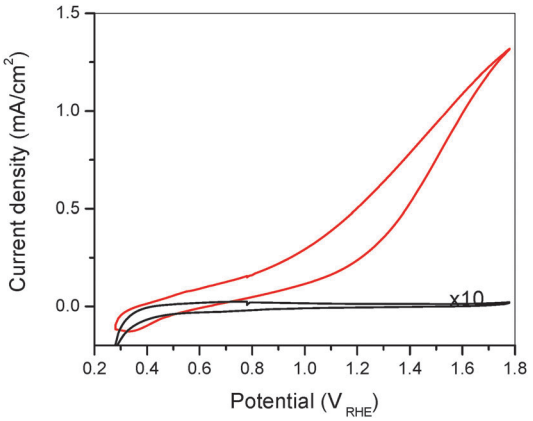

Fig. 1 Cyclic voltammograms (CVs) of the as-prepared $BiVO_4$ film electrode. Both the dark current (black) and the photocurrent under AM1.5 sunlight (red) are shown (front side illumination). The dark current data are amplified to show the absence of electrochemical water oxidation on $BiVO_4$ in the potential region.

The dark current for the as-prepared $BiVO_4$ film (Fig. 1) is close to zero until 1.80 V_{RHE}. The near-zero current in the dark indicates that the native surface of $BiVO_4$ cannot oxidize water efficiently (for a current density of 20 μA cm^{-2}) below an overpotential of 0.57 V. From the photocurrent curve of the as-prepared $BiVO_4$ electrode (Fig. 1), a current density of 0.54 mA cm^{-2} (0.27 mA cm^{-2}) at 1.23 V_{RHE} is obtained for the forward (reverse) scan. The onset potential is determined to be 0.40 V_{RHE} (0.65 V_{RHE}).

The electrochemical processes for loading and removal of NiO_x onto $BiVO_4$ are shown in Fig. 2A and B, respectively. The appearance of the oxidation–reduction peaks at 1.57 V_{RHE}/1.37 V_{RHE}, which are assigned to the oxidation–reduction of NiO_x, directly confirms a successful loading of NiO_x onto $BiVO_4$. During the loading process (Fig. 2A), the peak of NiO_x oxidation–reduction became more and more prominent as the electrode was electrochemically cycled between 0.50 V_{RHE} and 1.80 V_{RHE}. As a result of NiO_x loading, the potential bias needed for water oxidation decreased from 1.8 V_{RHE} to $<$1.6 V_{RHE}. The increased dark current after NiO_x-loading onto $BiVO_4$ agrees well with previous reports[16] which show that NiO_x can effectively catalyze water oxidation. After treating the NiO_x loaded $BiVO_4$ in 0.2 M NaP*i* electrolyte, the redox peak feature for $NiOOH/Ni(OH)_2$ disappears and the onset potential for water oxidation in the dark changes back to $>$1.8 V_{RHE} (Fig. 2B). The much decreased current density in the region of NiO_x oxidation–reduction in Fig. 2B compared to Fig. 2A is caused by a *chemical* removal of NiO_x using phosphate before the *electrochemical* removal of NiO_x could occur. The oxidation–reduction peak at 0.79 V_{RHE}/0.72 V_{RHE} becomes obvious after the electrochemical removal of NiO_x (Fig. 2B). This redox peak is tentatively assigned to the oxidation–reduction of tetrahedral coordinated VO_2^+/VO^{2+} species on the surface of $BiVO_4$, which is $\sim$0.20 V less anodic than the octahedrally coordinated VO_2^+–VO^{2+} redox couple in aqueous solution.[18] The NiO_x species loaded onto $BiVO_4$ are therefore suggested to cover some VO sites on the $BiVO_4$ surface

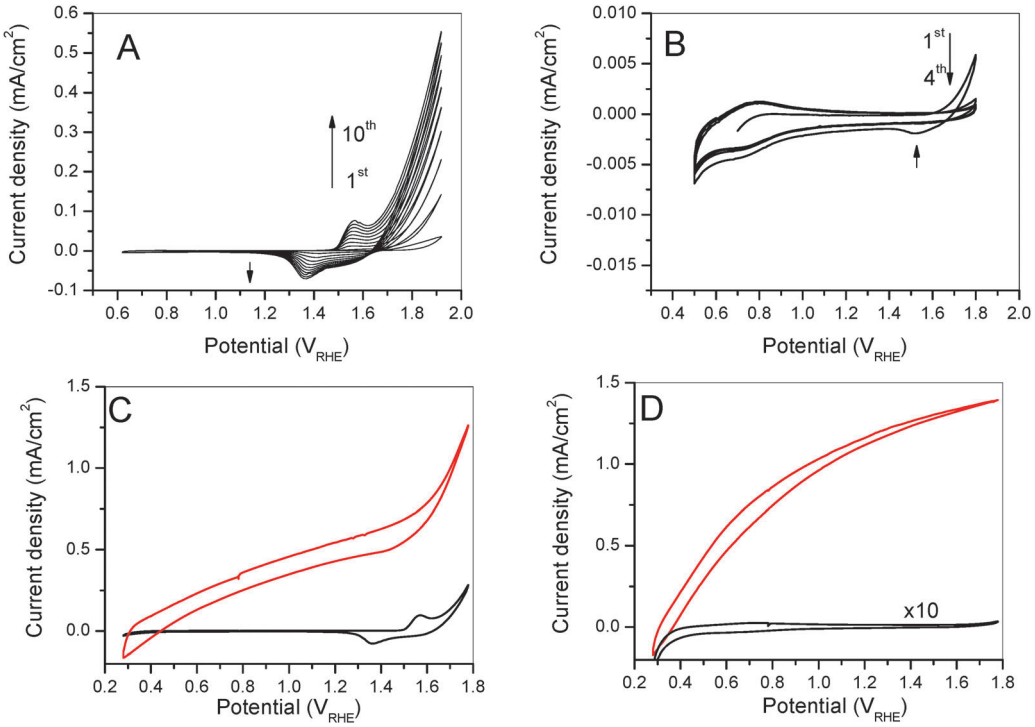

Fig. 2 (A) CVs for NiO_x loading onto $BiVO_4$ electrodes. A current density of ~0.1 mA cm^{-2} for the NiO_x oxidation peak (1.61 V_{RHE}) is typically obtained after 10 cyclic scans. (B) CVs for removal of NiO_x in phosphate buffer (pH = 7.0). The cyclic scan (from 0.5 V_{RHE} to 1.8 V_{RHE}) starts in the anodic direction. The current at >1.4 V_{RHE} drops close to zero during scanning, which indicates the removal of NiO_x OER catalytic centers. Typically 4 cycles were used to ensure a complete removal of NiO_x OER catalytic centers. (C) CVs of a $BiVO_4$ film electrode after electrochemical loading of NiO_x, and (D) CVs for the $BiVO_4$ film after removal of NiO_x OER centers. Both the dark current (black) and the photocurrent under the simulated AM1.5 sunlight for front side illumination (red) are shown. The dark current data in panel D are amplified to show the absence of NiO_x OER centers on $BiVO_4$.

and the removal of NiO_x OER centers using phosphate exposes these VO sites again. These VO_x species are proposed to be the OER centers for both the as-prepared $BiVO_4$ electrodes and the $BiVO_4$ electrodes that undergo the NiO_x loading and phosphate treatment processes.

The XPS spectra were recorded to verify the loading of the NiO_x centers onto the surface of the $BiVO_4$ photoelectrode and their subsequent removal in phosphate buffer. As shown in the literature,[19,20] V atoms at the surface are found to be partly leached out (V : Bi ratio <1). Therefore, the concentration of Ni on the surface is quantified through the ratio between Ni and Bi by using the amount of Bi as an internal reference. As summarized in Table 1, a high concentration of Ni (Ni : Bi = 5.96 : 1) was detected on the $BiVO_4$ surface after NiO_x loading in a borate electrolyte. After phosphate treatment, the ratio between Ni and Bi on the surface decreased to 0.59. The decrease of Ni content not only directly proves that the phosphate removes the loosely coordinated NiO_x-OER centers on the surface of $BiVO_4$, but also shows that a small fraction of more tightly bound Ni remains attached to the surface. Although the exact Ni : Bi ratio varies from 0.3 to 0.6, for different $BiVO_4$ samples after phosphate treatment, the XPS data do clearly demonstrate the partial removal of NiO_x from the surface of $BiVO_4$.

Table 1 The chemical composition on the surface of a series of $BiVO_4$ photoelectrodes at different stages for treatment

	As-prepared $BiVO_4$	NiO_x loaded $BiVO_4$, as deposited	NiO_x loaded $BiVO_4$, after phosphate treatment
Ni : Bi ratio	0.00 : 1	5.96 : 1	0.59 : 1
V : Bi ratio	0.94 : 1	0.48 : 1	0.40 : 1

Fig. 2C and D shows the effects of the NiO_x loading-and-removal process on the performance of the $BiVO_4$ photoelectrodes in a NaB*i* electrolyte (without Ni^{2+} in the solution). After electrochemical NiO_x loading onto the $BiVO_4$ electrode (shown in Fig. 2A), a dark-current is observed at >1.50 V_{RHE} for the $BiVO_4$ electrode (Fig. 2C). The current peak at 1.56 V_{RHE} is assigned to the oxidation of $Ni(OH)_2$ to NiOOH.[21] When the scan direction is reversed, a bump between 1.2 V_{RHE} and 1.5 V_{RHE} appears in the CV. The bump in the CV curve is assigned to the reduction of NiOOH to $Ni(OH)_2$. The peak positions are in agreement with the data shown in Fig. 2A. The >100 mV separation between the oxidation peak and the reduction peak indicates that the redox process is not reversible. The large widths of the oxidation–reduction peaks are related to the fact that multiple forms of $Ni(OH)_2$ (α-$Ni(OH)_2$ and β-$Ni(OH)_2$) and NiOOH (β-NiOOH and γ-NiOOH) which might also include Ni^{4+} species are involved during the oxidation–reduction.[22] The steep increase in the anodic current after NiO_x oxidation indicates that water oxidation occurs electrochemically in the dark. From the photocurrent curve for NiO_x loaded $BiVO_4$ (Fig. 2C), a current

density of 0.55 mA cm^{-2} (0.44 mA cm^{-2}) at 1.23 V_{RHE} is obtained for the forward (reverse) scan. The onset potential for the photocurrent is determined to be 0.31 V_{RHE} (0.45 V_{RHE}) for the forward (reverse) scan.

After the phosphate treatment of the NiO_x-loaded $BiVO_4$, the redox peak feature for NiOOH to $Ni(OH)_2$ disappears and the current in the dark is again close to zero up to 1.80 V_{RHE} (Fig. 2D). This suggests that any remaining Ni species is much less active for OER than the NiO_x species represented by the redox wave shown in Fig. 2C. On the other hand, the photocurrent at 1.23 V_{RHE} goes up to 1.18 mA cm^{-2} (1.13 mA cm^{-2}) for the forward (reverse) scan. The onset potential for the photocurrent becomes 0.31 V_{RHE} (0.37 V_{RHE}) for the forward (reverse) scan.

For $BiVO_4$ films lower anodic currents are generally observed during the reverse scan than for the forward scan, both in the dark and under illumination. For the as-prepared $BiVO_4$ films and the NiO_x-removed $BiVO_4$ films, the hysteresis in the dark CVs is mostly caused by charging and discharging of the double-layer capacitance. For the NiO_x-loaded $BiVO_4$ films, the hysteresis in the dark CVs is mainly due to the oxidation–reduction of NiO_x species. Since the O_2 molecules produced cannot desorb from the $BiVO_4$ surface fast enough, they will block the active OER sites on the $BiVO_4$ surface and cause further hysteresis for the $BiVO_4$ electrodes under high potential bias or sunlight illumination.

The effects of the NiO_x loading-and-removal process on the surface of $BiVO_4$ are also observed during the steady state characterization. The stabilized photocurrent at 1.23 V_{RHE} increased slightly from 0.34 mA cm^{-2} to 0.49 mA cm^{-2} after NiO_x loading, and then increased to 1.08 mA cm^{-2} after the removal of NiO_x (Fig. 3A). These values agree well with the photocurrent determined from the CVs shown in Fig. 2. The measurements at a long time scale (Fig. 3B) further show that the improvement in the photocurrent through the NiO_x loading-and-removal procedure persists at least for a time period of ~1 h. The photocurrent for the passivated $BiVO_4$ photoelectrode slowly decreased from 1.08 mA cm^{-2} to 0.91 mA cm^{-2} during the first 2200 seconds. The incubation of the $BiVO_4$ photoelectrode in the dark (from 2200 seconds to 2300 seconds) does not affect the photocurrent upon the next illumination. On the other hand, bubbling air through the electrolyte (during the dark period between 2700 seconds and 2900 seconds) changes the photocurrent back to 1.09 mA cm^{-2}. This suggests that the activity loss during the first 2200 seconds is caused by gas bubbles accumulated on the surface, which block the contact between the $BiVO_4$ electrode and the electrolyte. This proves that the effects of NiO_x loading/removal on the photocurrent are stable.

In contrast, the photocurrent does not increase over long-time characterization of the as-prepared $BiVO_4$ electrodes in 0.2 M NaP*i* (ESI,† Fig. S2). This demonstrates that the above described improvement is not simply caused by extra electrolysis in the presence of phosphate anions, but that rather a prior loading of NiO_x is required. It is also noted that the effects of the NiO_x loading-and-removal process on the surface of $BiVO_4$ are repeatable. A second loading of NiO_x onto the passivated $BiVO_4$ will change the CVs back into those shown in Fig. 2C and a following electrochemical removal of NiO_x OER centers from $BiVO_4$ in a NaP*i* electrolyte will recover the photocurrent as shown in Fig. 2D.

For employing $BiVO_4$ for solar fuel production in, for example, artificial leaf devices the high energy photons need to be absorbed by the water exposed $BiVO_4$ and the low energy photons need to be absorbed by a second material of lower band gap (such as Si). Considering this, front-side illumination was used above for the photocurrent collection from the $BiVO_4$ photoelectrodes. On the other hand, $BiVO_4$ photoelectrodes are known to perform better under back side illumination than under front side illumination due to the sluggish electron transport inside $BiVO_4$.[3,6] To allow direct comparisons with the performance of $BiVO_4$ reported earlier, the IPCE spectrum under back-side illumination for the $BiVO_4$ electrode (under the bias of 1.23 V_{RHE}) was collected (Fig. 4A) after the NiO_x-OER centers were removed. The IPCE steadily increases from zero at 510 nm to a plateau at ~440 nm,

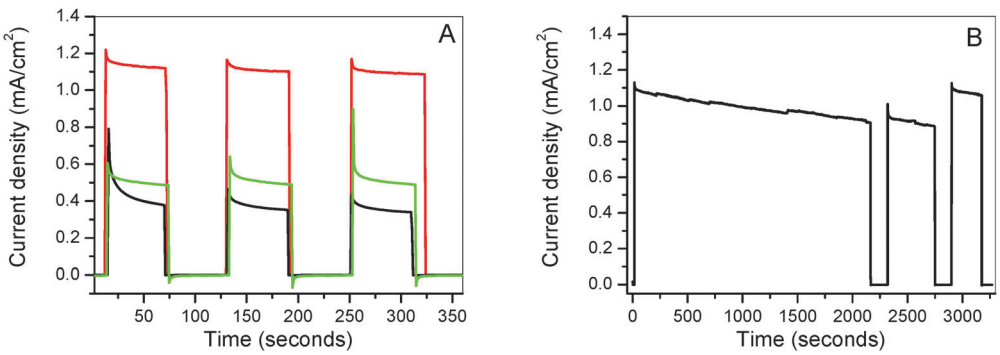

Fig. 3 Chronoamperometric characterization of the $BiVO_4$ electrodes biased at 1.23 V_{RHE}. (A) The as-prepared $BiVO_4$ film electrode (black), $BiVO_4$ film electrode after NiO_x loading (green), and $BiVO_4$ film electrode after electrochemical removal of NiO_x OER centers (red). The measurements started with the condition that the $BiVO_4$ electrode was kept in the dark, the white-light is chopped on and off approximately every 60 seconds. (B) Current–time trace for the passivated $BiVO_4$ electrode on a long-time scale. The measurement started in the dark. At 10 seconds, 2300 seconds and 2900 seconds, the shutter was opened. At 2200 seconds and 2700 seconds, the shutter was closed. Between 2700 seconds and 2900 seconds, air was passed through the electrolyte to remove the O_2 bubbles accumulated on the surface of the $BiVO_4$ electrode.

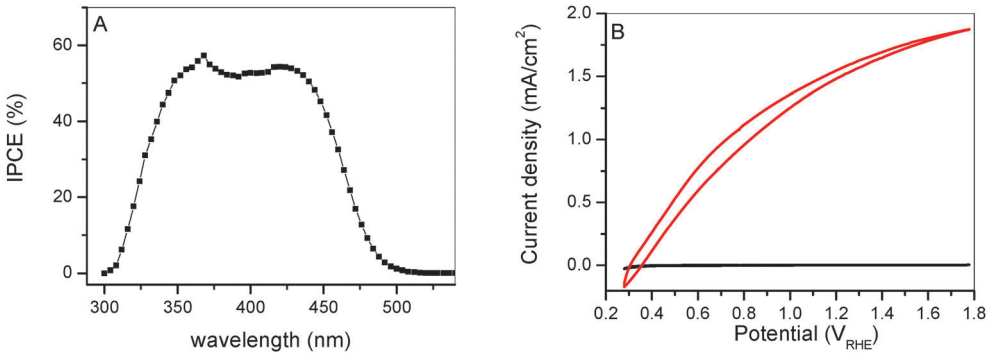

Fig. 4 (A) The IPCE spectrum of the $BiVO_4$ photoelectrode after NiO_x OER center removal (biased at 1.23 V_{RHE} in a 0.2 M NaB*i* electrolyte, under back side illumination). (B) The CVs of the same $BiVO_4$ photoelectrode in the dark (black), and under back side illumination (red).

and remains almost constant until it starts to decrease at ~350 nm. The decrease is due to the absorption of the photons by the FTO glass.[6] While the trend in the IPCE spectrum is similar to that reported previously,[6] the absolute values of IPCE increased significantly. The IPCE at 450 nm reaches 43% for the passivated $BiVO_4$ photoelectrode. By assuming that the IPCEs are independent of the light intensity, a photocurrent of 2.30 mA cm^{-2} is predicted for the same $BiVO_4$ photoelectrode under simulated sunlight by integrating the IPCE spectrum (collected at a low light intensity of ~10 μW cm^{-2}) over the standard AM1.5 sunlight (light intensity of 100 mW cm^{-2}) spectrum.[23]

The CVs of the same $BiVO_4$ electrode in the dark and under simulated AM1.5 sunlight (back side illumination) were also collected and are shown in Fig. 4B. At 1.23 V_{RHE}, a photocurrent of 1.57 mA cm^{-2} (1.51 mA cm^{-2}) is obtained. Two factors need to be considered before addressing the difference between the experimental value and the predicted value. Firstly, the $BiVO_4$ film only absorbs max. ~90% of the photons of wavelengths from 300 nm to 600 nm (Fig. S3, ESI†). Secondly, ~10% less photons for this spectral region than that for the corresponding AM1.5 spectrum are available to excite $BiVO_4$ photoelectrodes, due to the loss caused by the mirror in our setup (Fig. S1, ESI†). After taking these two factors into consideration, the photocurrent obtained under the simulated sunlight accounts for ~90% of the predicted value. The ~10% loss of the photocurrent for the $BiVO_4$ photoelectrode observed experimentally is attributed to the increased carrier recombination in the bulk[5] as the light intensity increases to 100 mW cm^{-2} (for AM1.5 sunlight).

Discussion

Our results can be summarized as follows: (i) the NiO_x loading onto $BiVO_4$ photoelectrodes only slightly increases the photocurrents at low biases, despite the fact that it does improve the OER kinetics in the dark; (ii) a subsequent treatment of NiO_x loaded $BiVO_4$ photoelectrodes in a phosphate electrolyte removes the NiO_x OER catalytic centers and effectively improves the photocurrent for the $BiVO_4$ photoelectrodes (Fig. 5A); and (iii) a small fraction of NiO_x remains bound to the surface after the NiO_x loading/depletion procedure.

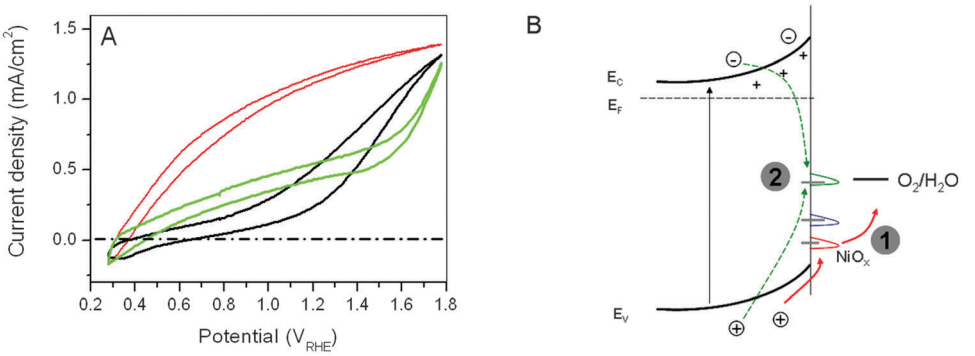

Fig. 5 (A) Comparison between the CVs for the $BiVO_4$ film electrode at various stages of treatment. For clarity, only the photocurrent curves from Fig. 1 and Fig. 2C and D are re-drawn. (Black) As-prepared $BiVO_4$ film, (green) $BiVO_4$ film after electrochemical loading of NiO_x, and (red) $BiVO_4$ film after removal of NiO_x OER centers. (B) The scheme shows the competing pathways for the photogenerated carriers at the $BiVO_4$–H_2O interface. Pathway 1 (red) represents the water oxidation by the holes and pathway 2 (green) represents the carrier recombination through a recombination center at the surface. Three types of surface states located at different energy levels inside the band gap of $BiVO_4$ are shown, catalytic center for OER (red), passivation center (blue), the recombination center (green). They are proposed to be generated upon NiO_x loading and to represent structurally different coordination environments. For the as-prepared $BiVO_4$ photoelectrodes and the $BiVO_4$ photoelectrodes to undergo the NiO_x loading and NiO_x OER center removal process, VO_x centers on the surface are proposed to be the OER centers.

To explain the results, the microscopic structure of the electrodeposited NiO_x is considered. The electrodeposited NiO_x is made of disorderly connected Ni–O cubes. At the edges of the NiO_x cluster, borate or phosphate is coordinated. The ability to remove NiO_x species, which are loaded in a NaB*i* electrolyte, by treatment with NaP*i* is rooted in the higher binding strength of phosphate to NiO_x than of borate to NiO_x. This is consistent with a recent report that borate favors larger-size NiO_x/CoO_x domains due to its weaker binding force than phosphate.[24]

The nanosized NiO_x domains are anchored to the surface of $BiVO_4$ *via* the dangling bonds from $BiVO_4$. Various coordination environments exist on the surface of $BiVO_4$ for the NiO_x species, and the amorphous nature of electrodeposited NiO_x[22] further allows the existence of various species with different coordination environments and/or valence states. As a result, heterogeneity in the NiO_x layer is almost unavoidable. The heterogeneity within the NiO_x layer is furthermore supported by the large widths of the oxidation–reduction peaks. Our present data suggest the presence of at least three different types of NiO_x species on the surface of $BiVO_4$: the OER catalytic centers, the recombination centers and the passivation centers (Fig. 5B).

Within the picture that three types of NiO_x centers exist on the surface of $BiVO_4$, the results we observed are explained as follows: the relatively poor performance of the as-prepared $BiVO_4$ photoelectrodes is mainly due to the native recombination centers (resulting from the dangling bonds) at the surface. The NiO_x loading onto $BiVO_4$ passivates the native recombination centers from $BiVO_4$, provides effective catalytic centers for OER and, unfortunately, also introduces new recombination centers. As a net result, the performance of the $BiVO_4$ electrodes improves only to a small extent and under some conditions can even decrease (data not shown) after NiO_x loading. Coordinating with phosphate anions under electrochemical conditions removes the NiO_x species that constitute the OER catalytic centers and the newly introduced recombination centers. On the other hand, the NiO_x passivation centers, which are proposed to coordinate to the surface more strongly than the other two species, remain at the $BiVO_4$ surface. The remaining fraction was confirmed by XPS (Table 1). As a result of the presence of NiO_x passivation centers, the photocurrent for the photoelectrodes is greatly improved after treating NiO_x loaded $BiVO_4$ film with phosphate anions.

On the surface of $BiVO_4$ electrodes, there is a kinetic competition between the transfer of holes to OER catalysts (then to H_2O molecules, pathway 1 in Fig. 5B) and the transfer of holes to surface states, which eventually recombine with trapped electrons (pathway 2 in Fig. 5B). The OER at the VO_x sites on the native $BiVO_4$ surface is a slow process, which is evidenced from the close-to-zero dark current up to 1.8 V_{RHE} presented in Fig. 1. An improved performance of $BiVO_4$ photoelectrodes can therefore be either due to an increase in the rate of hole transfer to NiO_x (and further to H_2O) or due to a decrease in the rate of hole transfer to the surface states. In a recent paper,[8] the suppression of surface recombination for $BiVO_4$ photoelectrodes was reported by accelerating the hole transfer to H_2O through loading of the OER catalyst. Our data, which were obtained after removing the NiO_x OER catalyst, demonstrate that the blocking of carrier transfer to the surface states leads to significant improvements in the performance of $BiVO_4$ photoelectrodes.‡

One referee proposes that a small remaining fraction of NiO_x after phosphate treatment may still become catalytically active for water oxidation under illumination. Due to the high driving force of the photoexcited holes at the valence band edge for $BiVO_4$, the remaining NiO_x centers, which are located at >1.9 V_{RHE}, do have the possibility to serve as the OER center in light, though they are not as active as the NiO_x center presented in Fig. 2C. However, the absence of dark-current (dark current in Fig. 1 and 2D) shows that the remaining NiO_x centers would be very inefficient OER catalysts, not significantly better than VO_x itself. As the photocurrents for the phosphate treated $NiO_x/BiVO_4$ electrode are much higher than those for the as-prepared $BiVO_4$ photoelectrode (Fig. 5A), it clearly demonstrates that the improvement is not due to the presence of the OER catalysts.

Conclusions

The passivation of the surface states between $BiVO_4$ and H_2O is achieved by electrochemical treatment of the NiO_x coated $BiVO_4$ electrodes in a phosphate electrolyte. This causes a passivation of surface states on $BiVO_4$ which in turn effectively improves the performance of photoelectrodes in the low-bias region. The heterogeneity of the NiO_x layer on $BiVO_4$ allows phosphate anions to selectively remove the two NiO_x species which serve as the OER catalytic centers and the carrier recombination centers, while the NiO_x centers that passivate the surface stays on the surface of $BiVO_4$. Identifying suitable OER catalysts or introducing a suitable interfacial layer that do not sacrifice the passivating effects reported here promises further improvement of $BiVO_4$ photoelectrodes.

Acknowledgements

The authors were supported by the Artificial Leaf Project Umeå (K&A Wallenberg foundation), the Solar Fuels Strong Research Environment Umeå (Umeå University), Vetenskapsrådet and the Swedish Energy Agency (Energimyndigheten). We thank Andrey Shchukarev for the XPS characterization and Hans-Martin Berends for stimulating discussions and comments to the manuscript.

‡ Note: During the reviewing process, a paper from Choi *et al.* was published.[25] Although both the $BiVO_4$ film and the NiO_x loading are different from ours, they also report that minimizing the carrier recombination at the interface is important for improving the performance of $BiVO_4$ photoelectrodes. An inert layer of FeOOH was found by them to passivate the interface thus effectively increasing the photocurrent. The two different methods to treat the $BiVO_4$ surface are now being researched in our lab for the elucidation of microscopic origins of the passivation.

References

1 F. F. Abdi, L. Han, A. H. M. Smets, M. Zeman, B. Dam and R. van de Krol, *Nat. Commun.*, 2013, **4**, 2195.
2 R. van de Krol, Y. Liang and J. Schoonman, *J. Mater. Chem.*, 2008, **18**, 2311.
3 Y. Park, K. J. McDonald and K. S. Choi, *Chem. Soc. Rev.*, 2013, **42**, 2321.
4 D. G. Nocera, *Acc. Chem. Res.*, 2012, **45**, 767.
5 F. F. Abdi and R. van de Krol, *J. Phys. Chem. C*, 2012, **116**, 9398.
6 Y. Liang, T. Tsubota, L. P. A. Mooij and R. van de Krol, *J. Phys. Chem. C*, 2011, **115**, 17594.
7 G. Wang, Y. Ling, X. Lu, F. Qian, Y. Tong, J. Z. Zhang, V. Lordi, C. Rocha Leao and Y. Li, *J. Phys. Chem. C*, 2013, **117**, 10957.
8 D. K. Zhong, S. Choi and D. R. Gamelin, *J. Am. Chem. Soc.*, 2011, **133**, 18370.
9 H. W. Jeong, T. H. Jeon, J. S. Jang, W. Choi and H. Park, *J. Phys. Chem. C*, 2013, **117**, 9104.
10 C. Ding, J. Shi, D. Wang, Z. Wang, N. Wang, G. Liu, F. Xiong and C. Li, *Phys. Chem. Chem. Phys.*, 2013, **15**, 4589.
11 S. K. Choi, W. Choi and H. Park, *Phys. Chem. Chem. Phys.*, 2013, **15**, 6499.
12 M. F. Lichterman, M. R. Shaner, S. G. Handler, B. S. Brunschwig, H. B. Gray, N. S. Lewis and J. M. Spurgeon, *J. Phys. Chem. Lett.*, 2013, **4**, 4188.
13 D. R. Gamelin, *Nat. Chem.*, 2012, **4**, 965.
14 B. Klahr, S. Gimenez, F. Fabregat-Santiago, J. Bisquert and T. W. Hamann, *J. Am. Chem. Soc.*, 2012, **134**, 16693.
15 M. Barroso, A. J. Cowan, S. R. Pendlebury, M. Grätzel, D. R. Klug and J. R. Durrant, *J. Am. Chem. Soc.*, 2011, **133**, 14868.
16 M. Dincã, Y. Surendranath and D. G. Nocera, *Proc. Natl. Acad. Sci. U. S. A.*, 2010, **107**, 10337.
17 T. Lindgren, H. Wang, N. Beermann, L. Vayssieres, A. Hagfeldt and S. E. Lindquist, *Sol. Energy Mater. Sol. Cells*, 2002, **71**, 231.
18 L. Li, S. Kim, W. Wang, M. Vijayakumar, Z. Nie, B. Chen, J. Zhang, G. Xia, J. Hu, G. Graff, J. Liu and Z. Yang, *Adv. Energy Mater.*, 2011, **1**, 394.
19 K. Sayama, A. Nomura, T. Arai, T. Sugita, R. Abe, M. Yanagida, T. Oi, Y. Iwasaki, Y. Abe and H. Sugihara, *J. Phys. Chem. B*, 2006, **110**, 11352.
20 C. Ding, J. Shi, D. Wang, Z. Wang, N. Wang, G. Liu, F. Xiong and C. Li, *Phys. Chem. Chem. Phys.*, 2013, **15**, 4589.
21 A. K. Shukla, S. Venugopalan and B. Hariprakash, *J. Power Sources*, 2001, **100**, 125.
22 D. K. Bediako, B. Lassalle-Kaiser, Y. Surendranath, J. Yano, V. K. Yachandra and D. G. Nocera, *J. Am. Chem. Soc.*, 2012, **134**, 6801.
23 AM1.5 sunlight spectrum, http://rredc.nrel.gov/solar/spectra/am1.5/, 2013.
24 C. L. Farrow, D. K. Bediako, Y. Surendranath, D. G. Nocera and S. J. L. Billinge, *J. Am. Chem. Soc.*, 2013, **135**, 6403.
25 T. W. Kim and K. S. Choi, *Science*, 2014, **343**, 990.

